Sine-modulated wavelength-independent full-range complex spectral optical coherence tomography with an ultra-broadband light source

Qiukun Zhang[1], Shuncong Zhong[1,2] and Jianfeng Zhong[1]

Abstract
We present a full-range complex spectral domain optical coherence tomography with an ultra-broadband light source based on sinusoidal modulation. For the sinusoidal modulation strategy, a lead zirconate titanate stack actuator is employed to achieve the sinusoidal vibration of a mirror and therefore to get a series of spectral interferogram with different phase delays. The purpose of this strategy is to get higher performance complex-conjugate artifact elimination. Bessel separation of the signal sequence at each wavelength of the spectrometer was used to reconstruct the real and imaginary components of interference fringes; however, the sinusoidal modulation method is independent of light source wavelength. The experimental results demonstrated that the method had an excellent performance in a complex-conjugate suppression of 50 dB for a *full width at half maximum* bandwidth of 236 nm, and it has better anti-artifact ability and more flexible range in phase shifting than the conventional wavelength-dependent phase-shifting method on a full-range complex spectral optical coherence tomography system. Furthermore, the effect of the hysteresis error of lead zirconate titanate actuators on the performance of complex-conjugate artifact elimination was investigated and the solution of lead zirconate titanate positioning performance for both conventional phase-shifting and sine-modulation methods was suggested.

Keywords
Sinusoidal phase modulation, complex-conjugate mirror error, spectral interferometry, optical coherence tomography

Introduction

Optical coherence tomography (OCT)[1] is a rapid developed imaging technology in the past 20 years.[2] It uses low-coherence light to unravel internal structure of examined objects. It can be used to analyze the interference signal between reflected and backscattered light from reference and sample beams to obtain images. In the last few years, the focus of new developments has shifted toward spectral domain optical coherence tomography (SD-OCT) and swept-source optical coherence tomography (SS-OCT) since it has been shown that these versions of OCT have huge advantages in terms of acquisition speed and sensitivity, as compared to time domain optical coherence

[1]Laboratory of Optics, Terahertz and Non-destructive Testing, School of Mechanical Engineering and Automation, Fuzhou University, Fuzhou, P.R. China
[2]Department of Naval Architecture, Ocean and Marine Engineering, University of Strathclyde, Glasgow, UK

Corresponding author:
Shuncong Zhong, Laboratory of Optics, Terahertz and Non-destructive Testing, School of Mechanical Engineering and Automation, Fuzhou University, Fuzhou 350108, P.R. China.
Email: zhongshuncong@hotmail.com

tomography (TD-OCT).[3–5] In SD-OCT, depth-resolved information is encoded in the frequency of the spectral density function recorded by a spectrometer and is retrieved by the Fourier transform.[6] Unfortunately, the SD-OCT image contains some parasitic elements, inherent to the technique, which obscure the images, especially the images of thick objects, requiring deep field of view. There are two reasons for this to happen. First, the original signal not only contains coherent components but also includes the direct current (DC) part and autocorrelation items. Second, what we used to describe as the interference fringes is a real function, and therefore, its Fourier transform is Hermitian; the reconstructed image is symmetrical about zero path difference. As a consequence, one cannot distinguish between negative and positive optical path differences with respect to the reference mirror.[7]

To resolve the problem, one can measure the phase of the spectral interferometer signal. An inverse Fourier transform of the complex data directly provides the true object structure, eliminating any mirror terms. To achieve the full-range complex spectral domain optical coherence tomography (FRCSD-OCT), several methods have been proposed. The first approach is to construct complex interference fringes by a phase-shifting method. The phase information required to reconstruct such a signal from intensity measurements is obtained from recording two to five spectra collected for a constant penetrating beam, but with the reference mirror being shifted by various fractions of wavelength of the light used.[8–10] In practice, such a result is difficult to achieve. Most of the methods require shifting the reference mirror by a precise fraction of the wavelength. If a relatively broadband light source is used, this leads to so-called polychromatic error[11] since the condition is only fulfilled for one wavelength. Most of the light sources used in the above researches were generally superluminescent diode (SLD) with a central wavelength of ~820 nm and a bandwidth of ~20 nm. The light sources have narrow bandwidth, and therefore, the polychromatic error caused is relatively small. However, if a broadband light source is employed, the polychromatic error will become obvious; also, the performance in the suppression of complex-conjugate artifacts will be deteriorated. Lippok et al.[12] used the Pancharatnam–Berry phase as a multifunctional tool for low-coherence interferometry. The geometric phase shift enables instantaneous retrieval of the quadrature components of the complex interferometric signal and allows for a complex-conjugate suppression of 40 dB for an optical bandwidth of 115 nm. Carrier-frequency-based technique is another method to reconstruct the complex interference fringes;[13–15] a tilted reference mirror or a reflective grating was used to generate a spatial carrier-frequency into the two-dimensional (2D) spectral interferogram registered in parallel FD-OCT. However, the

nonlinear spatial extension of the light degrades the suppression ratio of the complex-conjugate artifact. There is still a BM-scanning method for full-range complex Fourier domain OCT.[16,17] For those methods, the phase modulation of a reference beam (M-scan) and transversal scanning (B-scan) are simultaneously performed. It requires only a single A-scan for each single transversal position to obtain a full-range FD-OCT image. It can achieve high imaging speed but with low imaging quality, especially the lateral structure of the object changes fast. Moreover, a modified phase-shifting method based on the integrating bucket of sinusoidal phase modulation of the reference arm is also proposed,[18,19] and it requires a complex quadrature projection algorithm to compensate for the chromaticity and any phase variations between integrating bucket acquisitions.

In this article, we employed sinusoidal modulation strategy in a full-range complex spectral OCT system with a broadband white light source to get high-performance complex-conjugate artifact elimination. Bessel separation of the signal sequence at each wavelength of the spectrometer is used to reconstruct the real and imaginary components of interference fringes. After inverse Fourier transform of interference fringes, a double range and low-noised image will be obtained. We present the method, a detailed signal processing, and demonstrate the performance of the home-made system for a 10-layer polymer sample. It showed that the method has an excellent performance in suppression ratio of the complex-conjugate artifact, and it has better anti-artifact ability than the conventional phase-shifting method on a full-range complex spectral OCT system with a broadband white light source.

Full-range complex spectral OCT methods

The SD-OCT is based on low-coherent interference of a light. A parallel beam originating from the light source was split into two beams by a beam splitter: one penetrates along the z-axis of samples and was reflected back from the nth interface between structural layers with the delay of τ_n; the second beam was reflected from the reference mirror with the delay of τ_r. The interference fringes (described by $G'(k)$) were recorded as a function of frequency by a spectrometer as

$$
\begin{aligned}
G'(k) = G_{rr}(k) + \sum_n G_{nn}(k) \\
+ 2Re\left\{ \sum_{n \neq m} G_{nm}(k) \exp[-j4\pi k(\tau_n - \tau_m)] \right\} \\
+ 2Re\left\{ \sum_n G_{nr}(k) \exp[-j4\pi k(\tau_n - \tau_r)] \right\}
\end{aligned}
\tag{1}
$$

where $G(k)$ is the cross-spectral density function of source. The first two terms of equation (1) describe intensities of the light reflected back from the reference mirror and from layers within the object (DC of background). The third term corresponds to the mutual interference among the each layer within the object (autocorrelation noise). The last one originates from interference between mirror and layers within the object. Applying the inverse Fourier transform to equation (1), one can obtain

$$FFT^{-1}\{G'(k)\} = \Gamma_{rr}(\tau) + \sum_n \Gamma_{nn}(\tau)$$
$$+ \sum_{n \neq m} \Gamma(\tau \pm (\tau_n - \tau_m)) + \sum_n \Gamma(\tau \pm (\tau_r - \tau_n)) \quad (2)$$

where $\Gamma(\tau)$ is defined as temporal coherence function of source. $G(k)$ and $\Gamma(\tau)$ constitute a Fourier transform pair. Equation (2) is a function of τ, and it consists of several peaks positioned at $\tau = 0$, $\pm(\tau_n - \tau_m)$, and $\pm(\tau_r - \tau_n)$. The term $\tau = 0$ emerges because of the direct current background, while the term $\tau = \pm(\tau_n - \tau_m)$ originates from the self-coherent noise. Only the terms at $\tau = \tau_r - \tau_m$ provide the useful information which can be used to characterize the examined sample. The term $\tau = -(\tau_r - \tau_n)$ is the complex-conjugate mirror because $G'(k)$ is a real function.

Phase-shifting full-range complex spectral OCT method

In a conventional phase-shifting full-range complex spectral OCT system, the lead zirconate titanate (PZT) is generally used to drive the reference mirror by various fractions of wavelength of the light between each A-scan. They are three-phase, four-phase, and five-phase shifting methods. Better results on complex-conjugate removal could be achieved by taking up five A-scans.[20]

For the five-phase shifting method, the spectrometer records the spectral intensity function as I_1, I_2, I_3, I_4, and I_5. The complex interference fringes $\tilde{G}(k)$ can be calculated as follows

$$\phi(k) = \arctan \frac{2[I_2(k) - I_4(k)]}{2I_3(k) - I_5(k) - I_1(k)} \quad (3)$$

$$\varphi(k) = \frac{1}{4}\left(\{2[I_2(k) - I_4(k)]\}^2 + [2I_3(k) - I_5(k) - I_1(k)]^2\right)^{1/2} \quad (4)$$

$$\tilde{G}(k) = \varphi(k) \exp(i\phi(k)) \quad (5)$$

where $\phi(k)$ and $\varphi(k)$ are the phase and amplitude of complex interference fringes $\tilde{G}(k)$. In theory, the phase of $I_i(k)$ ($i = 1, 2, 3, 4, 5$) should be changed $\pi/2$ precisely for every wave number k. However, in a real OCT system, broadband source is generally used in order to obtain high axial resolution which results in most wavelengths of the light beam not meeting the requirements of the phase polarization. It therefore leads to the so-called polychromatic error. The broader the bandwidth of the light source, the larger the polychromatic error.

For the three-phase shifting method, when the phase-shifting interval is $2\pi/3$, the complex interference fringes $\tilde{G}(k)$ can be calculated as

$$\tilde{G}(k) = (3I_2(k) - 3I_3(k) - 2I_2(k)) + i * \sqrt{3}(I_2(k) + I_3(k)) \quad (6)$$

For the four-phase shifting method, the phase-shifting interval is $\pi/2$, and the complex interference fringes $\tilde{G}(k)$ can be calculated as

$$\tilde{G}(k) = (I_1(k) - I_3(k)) + i * (I_2(k) - I_4(k)) \quad (7)$$

In summary, the above phase-shifting methods are wavelength-dependent. The phase-shifting interval should be changed $\pi/2$ precisely for five-phase and four-phase shifting methods, while the phase-shifting interval is $2\pi/3$ for the three-phase shifting method.

Sinusoidal phase modulation method

To eliminate the unwanted terms and to construct a complex function of interference fringes, a sinusoidal phase modulation interferometer technology is employed in our SD-OCT system. An ultra-high precision closed-loop PZT actuator is used to drive the mirror for achieving sinusoidal vibration. Now a sinusoidal phase modulation term is added in interference fringes. The signal obtained by spectrometer can be described as

$$G'(k, t) = G_{rr}(k) + \sum_n G_{nn}(k)$$
$$+ 2Re\left\{\sum_{n \neq m} G_{nm}(k) \exp[-j4\pi k(\tau_n - \tau_m)]\right\} \quad (8)$$
$$+ 2Re\left\{\sum_n G_{nr}(k) \exp[-j4\pi k(\tau_n - \tau_r + \tau(t))]\right\}$$

where $\tau(t) = b * \sin(2\pi f_c t + \theta)$, b is the amplitude of the vibration, f_c is the modulation frequency, and θ is initial phase of the vibration. The first three parts of equation (8) are independent of position of mirror; they are constants with time (described by G_0). Applying Fourier transform to $G'(k, t)$, the following equation can be obtained

$$\begin{aligned} F(k, w) &= \text{FFT}_{(t)}\{G'(k, t)\} \\ &= G_0\delta(w) + 2\sum_n G_{nr}(k)\cos[4\pi k(\tau_n - \tau_r)] \times \\ &\quad \left[\sum_{m=-\infty}^{\infty}(-1)^m A_{2m}\delta(w - 2mw_c)\right] \\ &\quad + 2\sum_n G_{nr}(k)\sin[4\pi k(\tau_n - \tau_r)] \times \\ &\quad \left[\sum_{m=-\infty}^{\infty}(-1)^m A_{2m-1}\delta(w - (2m-1)w_c)\right] \end{aligned} \tag{9}$$

where m is an integer, $A_m = J_m(d)\exp(jm\theta)$, J_m is the nth order Bessel function, $\delta(w)$ is the Dirac function, $d = 4\pi kb$, $w = 2\pi f$, and $w_c = 2\pi f_c$. Equation (9) can be solved to get a complex function

$$\begin{aligned} &\text{Re}\left\{\sum_n G_{nr}(k)\exp(-j4\pi k(\tau_n - \tau_r))\right\} \\ &= \sum_n G_{nr}(k)\cos[4\pi k(\tau_n - \tau_r)] \\ &= \frac{Re\{F(k, 2n*w_c)\}}{2J_{2n}(d)\cos(2n*\theta)} \end{aligned} \tag{10}$$

$$\begin{aligned} &\text{Im}\left\{\sum_n G_{nr}(k)\exp(-j4\pi k(\tau_n - \tau_r))\right\} \\ &= \sum_n G_{nr}(k)\sin[4\pi k(\tau_n - \tau_r)] \\ &= \frac{-\text{Im}\{F(k, (2n-1)*w_c)\}}{2J_{2n-1}(d)\cos((2n-1)*\theta)} \end{aligned} \tag{11}$$

where $F(k, n*w_c)$ means Fourier spectrum of $G'(k, t)$ for n times of fundamental frequency ($n = 1, 2, \ldots$). Now the complex interference fringes $\tilde{G}(k)$ can be reconstructed as

$$\begin{aligned} \tilde{G}(k) &= \sum_n G_{nr}(k)\cos[4\pi k(\tau_n - \tau_r)] \\ &\quad + j\sum_n G_{nr}(k)\sin[4\pi k(\tau_n - \tau_r)] \\ &= \text{Re}\left\{\sum_n G_{nr}(k)\exp(-j4\pi k(\tau_n - \tau_r))\right\} \\ &\quad + j\text{Im}\left\{\sum_n G_{nr}(k)\exp(-j4\pi k(\tau_n - \tau_r))\right\} \end{aligned} \tag{12}$$

After applying inverse Fourier transform to equation (12), the chromatogram of inner structure of object can be obtained

$$\tilde{\Gamma}(\tau) = \text{FFT}^{-1}\{\tilde{G}(k)\} = \sum_n \Gamma(\tau - (\tau_r - \tau_n)) \tag{13}$$
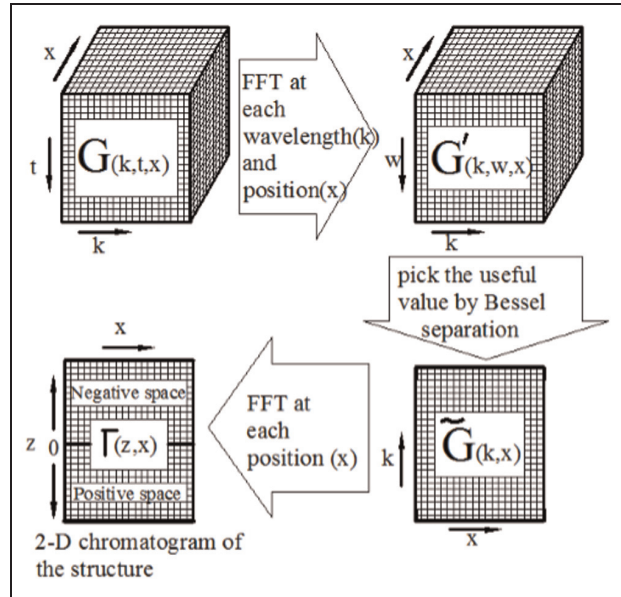

Figure 1. The detailed signal processing algorithm to achieve full-range complex OCT by sine-modulation strategy.

The detailed signal processing algorithm to achieve full-range complex OCT by sine-modulation strategy is shown in the flow chart in Figure 1.

It is worthy to note that the sinusoidal modulation method is independent of light source wavelength. It does not need precise phase-shifting interval like three-, four-, and five-phase shifting methods which in fact are wavelength-dependent.

Experiment

The basic components of a sine-modulated full-range complex spectral OCT system are shown as Figure 2.

A 50 W tungsten halogen lamp is used as the low-coherence broadband light source of the developed OCT system. The light from the lamp is delivered into a Michelson interferometer using a biconvex lens. Light is then split into reference and sample beams by a beam splitter (50/50). The light was focused to a 200 μm diameter spot on the sample and the reference mirror. Therefore, 200 μm is the lateral resolution of the developed OCT system which is possible to perform 2D OCT imaging, such as for non-destructive testing (NDT) of thermal barrier coatings and glass-fiber reinforced plastic (GFRP) materials. Both the backscattered lights from the sample and the mirror travel back toward the beam splitter and are finally collected by a broadband CCD-based spectrometer (USB2000 + ; Ocean Optics, USA). The spectrometer works in a wide range from 594.5 to 1028 nm with a high spectral resolution of 0. 2 nm. Interference occurs when both the
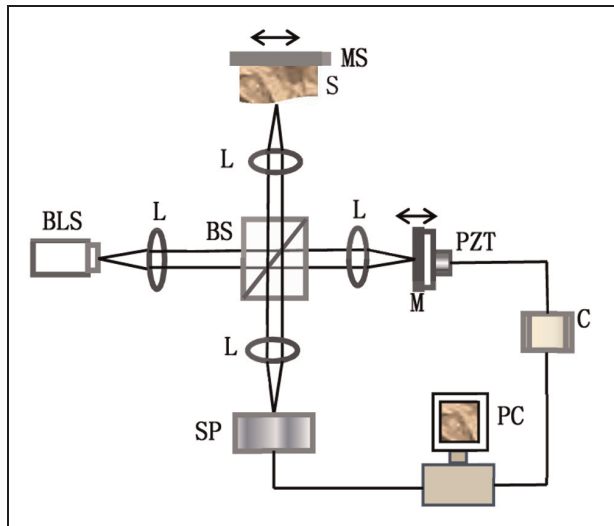
Figure 2. Experimental configuration of sine-modulated full-range complex spectral OCT.
BLS: broadband light source; L: lens; BS: beam splitter; S: sample; MS: moving stage; M: mirror; C: closed-loop controller; SP: spectrometer; PZT: lead zirconate titanate stack actuator.
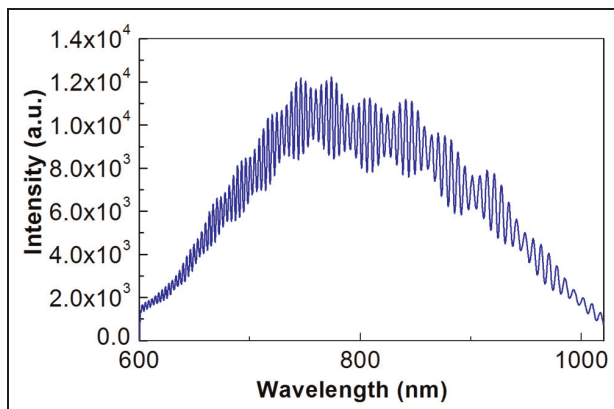

Figure 3. OCT spectral interferogram.

two beams are spatially matched in size and orientation, and their optical path lengths are matched within the coherence length of the light source. Figure 3 shows the typical OCT spectral interferogram obtained by spectrometer. For our current setup, the central wavelength is $\lambda_0 = 752$ nm, and full width at half maximum (FWHM) bandwidth is $\Delta\lambda = 236$ nm, corresponding to a measured axial resolution of ~ 1.1 μm (in air) calculated by the formula $2\ln2 * (\lambda_0)^2/(\pi * \Delta\lambda)$.[1] The simple sample here is a 10-layer polymer film which is used to compare the performance of complex-conjugate artifact elimination using five-phase shifting and sine-modulated methods. However, it does not mean that the developed OCT system could only be used to characterize the sample with clear interface layers. Like

other traditional OCT systems, the developed system could also be used for characterization of optical scattering media.

For the sinusoidal modulation strategy, a PZT stack actuator (Thorlabs) is employed to achieve the sinusoidal vibration of a mirror and therefore to get a series of spectral interferogram with different phase delays. The PZT accurately produces sine vibrations by a closed-loop controller. The sinusoidal PZT motion control is performed using a home-made software written in C++ . The spectrometer records a series of spectral interferogram while the mirror vibrates. Using equations (10) and (11), we obtain the useful information by dividing the value of the Bessel function. The reconstructed complex interference fringes $\tilde{G}(k)$ in equation (12) are greatly affected by the value of the Bessel function which is related to the vibration amplitude. After some experimental investigations, we suggest that the suitable vibration amplitude could be in the range of 100–180 nm. In this case, we selected the parameters of vibration function $\tau(t) = b * sin(2\pi f_c t + \theta)$, where vibration amplitude $b = 160$ nm, vibration frequency $f_c = 30$ Hz, and initial phase angle $\theta = 0$. The interference spectroscopy is acquired in the high-speed mode (integration time of 1 ms) using the current spectroscopy. It only takes about 33 ms to obtain all the spectral interferogram for a sinusoidal vibration. The corresponding computation can be achieved only in few microseconds.

Results and discussions

When a series of OCT spectral interferogram were obtained during the sinusoidal vibration of PZT, we rearrange the spectral interferogram along the time axis. We applied Fourier transform along the time axis to pick up the amplitude of multiple harmonics. After dividing the coefficient provided by the Bessel function, the real and imaginary components of interference fringes can be reconstructed. Figure 4 demonstrates the reconstructed real and imaginary components of interference fringes. A clear and full-depth tomography can be obtained after applying inverse Fourier transform of the reconstructed signals.

Figure 5 shows the imaging results of a single-point measurement on a two-layer sample. Figure 5(a) shows the result of conventional five-phase polarization complex spectral method, and Figure 5(b) shows the result of sine-modulated full-range complex spectral method. From the figures, it can be found that no DC background and autocorrelation item noise appear, and therefore, the two methods have good performance in dealing with DC background and autocorrelation item noise. For the conventional five-phase polarization method, there still is one obvious complex-conjugate
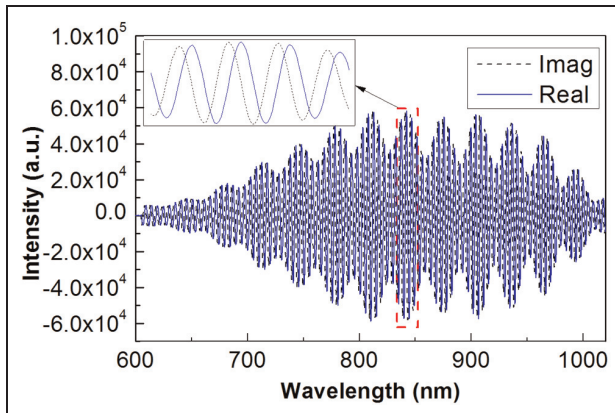
Figure 4. The reconstructed real (solid line) and imaginary (dashed line) components of interference fringes. The inset is the zoom view of the reconstructed signal in the dashed rectangle.
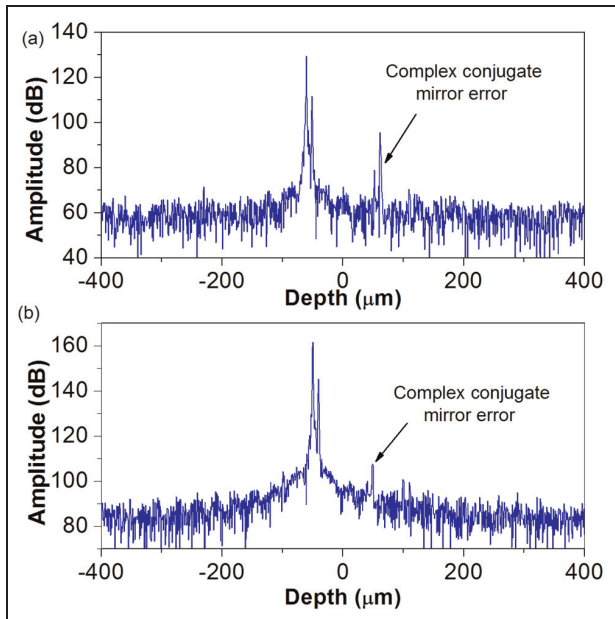

Figure 5. Results of (a) conventional five-phase shifting full-range complex spectral method and (b) sine-modulated full-range complex spectral method based on a single-point measurement.

mirror error compared with the noise background. However, the complex-conjugate mirror error almost submerged in the background using the sine-modulated full-range complex spectral method. Here, the ratio of the wanted signal and its complex-conjugate mirror signal as complex-conjugate mirror image suppression ratio (CCMISR) is defined to demonstrate the ability of complex-conjugate artifact elimination. Figure 6 shows comparison of the suppression ratio of complex-conjugate mirror image by conventional five-phase

shifting and sine-modulated full-range complex spectral methods for up to 100 experiments. The suppression ratio using sine-modulation strategy is about 50 dB, which is better than that of the five-phase shifting method of about 20 dB. It means that a sine-modulated FRCSD-OCT has better complex-conjugate artifact elimination ability and can detect more subtle change in the object when full-depth imaging is realized.

In order to make further investigation on the complex-conjugate artifact elimination ability, a 10-layer polymer thin film was measured by using the five-phase shifting and sine-modulated FRCSD-OCT methods. Figure 7(a) and (b) show the 2D OCT images obtained by conventional five-phase shifting method and sine-modulation methods. Figure 7(c) shows the scanning electron microscopy (SEM) image of the sample which is used to calibrate the OCT results. It can be seen from the figures that the two methods clearly and accurately detect the internal structure of the multi-layered polymer sample. However, the image of the conventional five-phase shifting method still has mirror trace residues, which is the mirror of surface, as indicated by an arrow in Figure 7(a). For the sine-modulated method, mirror trace residues have nearly been eliminated, as shown in Figure 7(b). Therefore, it has been demonstrated that the sine-modulated FRCSD-OCT has a better performance than five-phase shifting FRCSD-OCT in complex-conjugate artifact elimination.

As mentioned previously, for an OCT system with broadband light sources, the polychromatic error gets more obvious with increase in the bandwidth of light sources. The FWHM bandwidth $\Delta\lambda = 236$ nm of our current setup is relatively broader than the light used in phase-shifting methods,[7–10] and therefore, the larger complex-conjugate artifact is inherent to the technique.

On the other aspect, the reference mirror is generally driven by a PZT. The phase shifting for the five-phase shifting method is 0, $\pi/2$, π, $3\pi/2$, and 2π. For our light source with central wavelength of 752 nm, five-phase shifting of 0, 188, 376, 564, and 752 nm is needed to implement the five-phase shifting method. Compared with the conventional five-phase shifting method, only small shifting (e.g. $b = 160$ nm) is used in the sine-modulated method. Therefore, the sine-modulated method is independent of light source wavelength, and it has more flexible range in phase shifting than the conventional wavelength-dependent phase-shifting method.

Figure 8 shows the dynamic hysteretic behavior of PZT in the experiment, which is measured by home-made optical coherence vibration tomography system.[21] The hysteretic curve of PZT was carried out by varying the input voltage on the whole range in the ascending and descending directions. The dashed line denotes the input voltage from 0 to 30 V in the ascending and
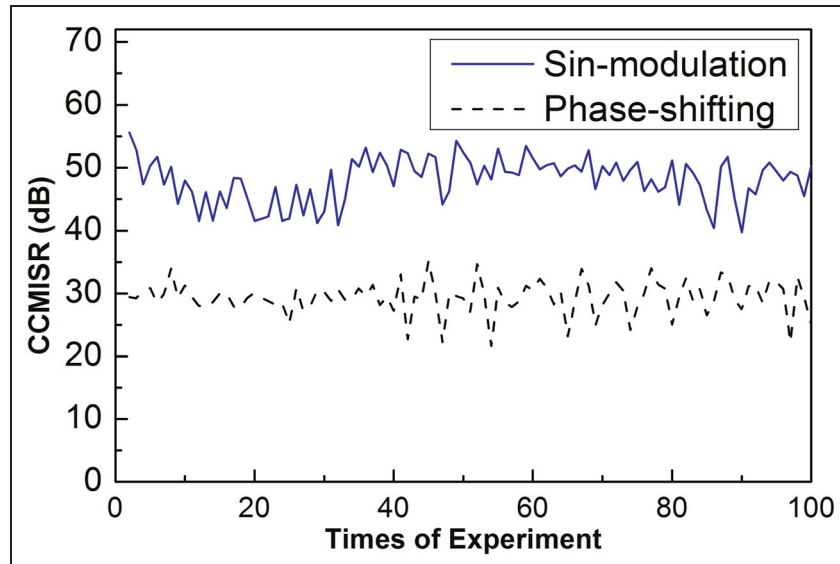
Figure 6. Comparison of the suppression ratio of complex-conjugate mirror image by conventional five-phase shifting and sine-modulated full-range complex spectral methods: the solid and dashed lines denote sine-modulation and phase-shifting methods, respectively.
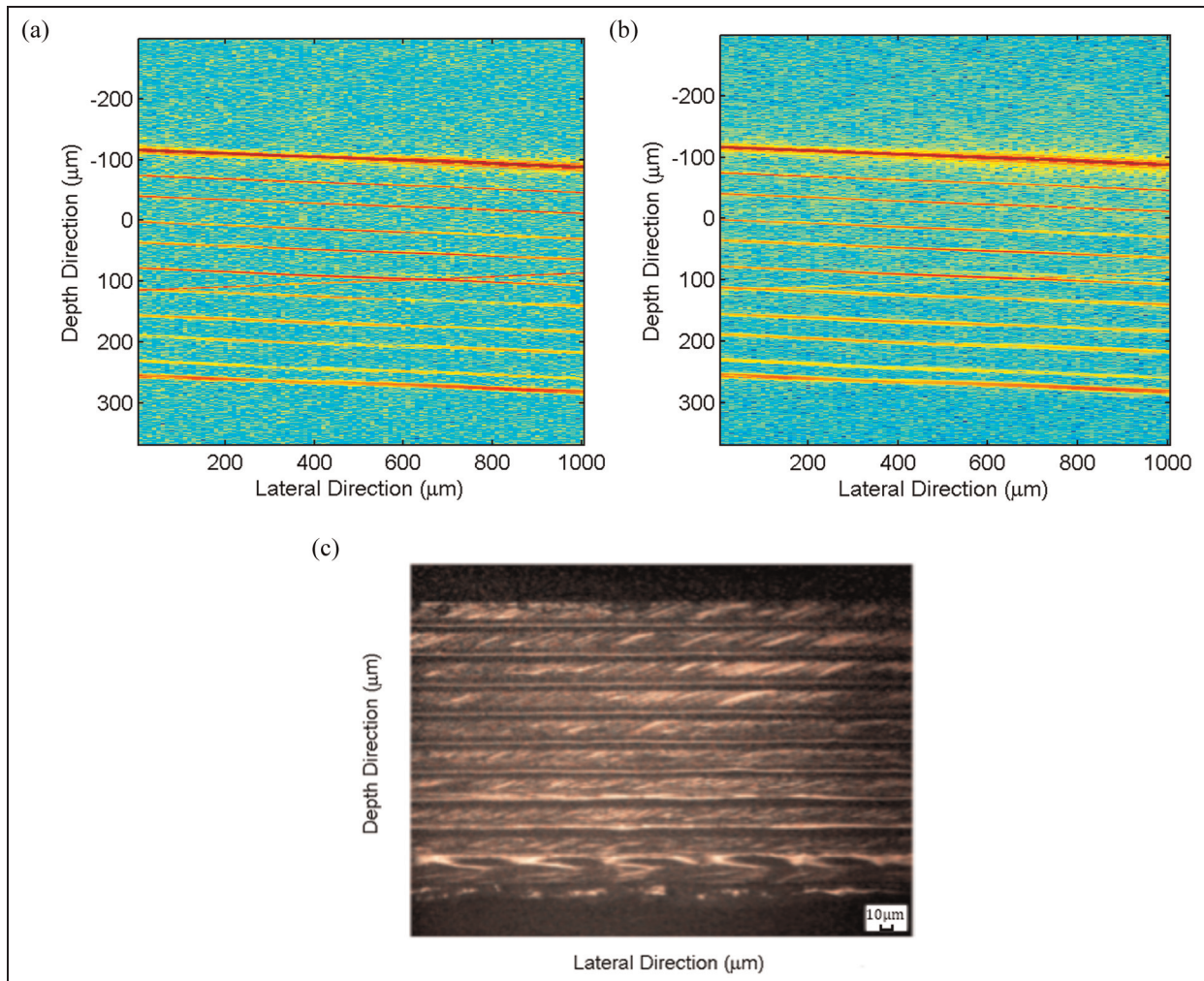

Figure 7. Two-dimensional OCT images by (a) conventional five-phase shifting and (b) sine-modulated methods; (c) SEM image of a 10-layer polymer film. The arrow in (a) indicates the mirror trace residues for the five-phase shifting method.
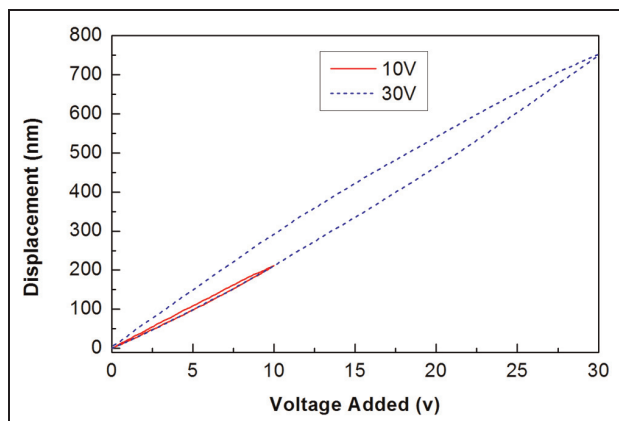
Figure 8. Dynamic hysteretic behavior of PZT: the dashed line denotes the input voltage from 0 to 30 V in the ascending and descending directions; the solid line denotes the input voltage from 0 to 10 V in the ascending and descending directions.

descending directions, while the solid line denotes the input voltage from 0 to 10 V in the ascending and descending directions. The hysteretic behavior of PZT can be used to explain the performance comparison between the two methods. Ideally, if precise five-phase shifting can be achieved, the performance of five-phase shifting method in complex-conjugate artifact elimination will be perfect. However, the performance of the five-phase shifting will be affected by the hysteresis error of PZT used. From Figure 8, it can be seen that there is larger hysteresis error when the displacement shifting is larger. For example, the hysteresis error is about 3.5 nm when the shifting is 752 nm, while it is about 0.2 nm for the shifting of 160 nm. The larger hysteresis error for the five-phase shifting method results in the poor performance of complex-conjugate artifact elimination, as shown in Figure 7(a). More recently, a precision control method based on hysteresis model[22] was proposed to significantly improve the positioning precision of piezoelectric actuators. The method could contribute to enhance the PZT positioning performance for both five-phase shifting method and the sine-modulation method. Furthermore, for the real application, the speed of sine modulation is to be considered since it needs more time than the five-phase shifting method.

In the field of mechanical engineering, the developed OCT system provides a potential NDT tool for evaluation of GFRP materials, thermal barrier coatings, and multi-layered thin film structures. In theory, a higher speed sinusoidal vibration strategy and a higher speed spectroscopy will lead to faster imaging. However, in order to implement real-time 2D OCT imaging, the availability of an ultrahigh-speed spectroscopy and a high-speed sample scanning device will be an issue which will be considered as our future work.

Conclusion

An FRCSD-OCT method based on sinusoidal phase modulation is presented for complex-conjugate artifact elimination. Bessel separation of the signal sequence at each wavelength of the spectrometer is used to reconstruct the real and imaginary components of interference fringes. After inverse Fourier transform of interference fringes, a double range and low-noised image will be obtained. The sinusoidal modulation method is independent of light source wavelength, and it has an excellent performance in a complex-conjugate suppression of 50 dB for a FWHM bandwidth of 236 nm. The experimental results demonstrated that the sinusoidal modulation method has better anti-artifact ability than the conventional wavelength-dependent phase-shifting method on a full-range complex spectral OCT System. However, for real applications, the speed of sine modulation is to be considered. The effect of hysteresis error of PZT actuator on the performance of complex-conjugate artifact elimination was discussed, and the solution of PZT positioning performance for both five-phase shifting and sine-modulation methods was suggested as well.

Declaration of conflicting interests

The authors declare that there is no conflict of interest.

Funding

References

1. Huang D, Swanson E, Lin C, et al. Optical coherence tomography. *Science* 1991; 254: 1178–1181.
2. Fercher A, Drexler W, Hitzenberger C, et al. Optical coherence tomography—principles and applications. *Rep Prog Phys* 2003; 66: 239.
3. Leitgeb R, Hitzenberger C and Fercher A. Performance of Fourier domain vs time domain optical coherence tomography. *Opt Express* 2003; 11: 889–894.
4. Hsu J, Lu C, Deng C, et al. Optical coherence tomography using nonlinear optics in fiber for broadband source generation. *Opt Commun* 2002; 212: 391–396.
5. Choma M, Sarunic M, Yang C, et al. Sensitivity advantage of swept source and Fourier domain optical coherence tomography. *Opt Express* 2003; 11: 2183–2189.

6. Fercher A, Hitzenberger C, Kamp G, et al. Measurement of intraocular distances by backscattering spectral interferometry. *Opt Commun* 1995; 117: 43–48.

7. Fercher A, Leitgeb R, Hitzenberger C, et al. Complex spectral interferometry OCT. *Proc SPIE* 1999; 3564: 173.

8. Targowski P, Wojtkowski M, Kowalczyk A, et al. Complex spectral OCT in human eye imaging in vivo. *Opt Commun* 2004; 229: 79–84.

9. Targowski P, Gorczynska I, Szkulmowski M, et al. Improved complex spectral domain OCT for in vivo eye imaging. *Opt Commun* 2005; 249: 357–362.

10. Wang K. *In vivo* full range complex Fourier domain optical coherence tomography. *Appl Phys Lett* 2007; 90: 054103.

11. Szkulmowski M, Bajraszewski T, Szkulmowska A, et al. Efficient residual error reduction in complex spectral optical coherence tomography with arbitrary or unknown phase. *Opt Appl* 2006; 36: 147.

12. Lippok N, Coen S, Leonhardt R, et al. Instantaneous quadrature components or Jones vector retrieval using the Pancharatnam-Berry phase in frequency domain low-coherence interferometry. *Opt Lett* 2012; 37: 3102–3104.

13. Leitgeb R, Michaely R, Lasser T, et al. Complex ambiguity-free Fourier domain optical coherence tomography through transverse scanning. *Opt Lett* 2007; 32: 3453–3455.

14. Huang B, Bu P, Nan N, et al. Single-shot parallel full range complex Fourier-domain optical coherence tomography. *J Phys Conf Ser* 2011; 277: 012015.

15. Bu P, Wang X and Sasaki O. One-shot parallel complex Fourier-domain optical coherence tomography using a spatial carrier frequency. *Opt Eng* 2008; 47: 050502.

16. Jaillon F, Makita S, Yabusaki M, et al. Parabolic BM-scan technique for full range Doppler spectral domain optical coherence tomography. *Opt Express* 2010; 18: 1358–1372.

17. Yasuno Y, Makita S, Endo T, et al. Simultaneous B-M-mode scanning method for real-time full-range Fourier domain optical coherence tomography. *Appl Opt* 2006; 45: 1861–1865.

18. Tao Y, Zhao M and Izatt J. High-speed complex conjugate resolved retinal spectral domain optical coherence tomography using sinusoidal phase modulation. *Opt Lett* 2007; 32: 2918–2920.

19. Wang K, Ding Z, Zeng Y, et al. Sinusoidal B-M method based spectral domain optical coherence tomography for the elimination of complex-conjugate artifact. *Opt Express* 2009; 17: 16820–16833.

20. Köttig F, Cimalla P, Gartner M, et al. An advanced algorithm for dispersion encoded full range frequency domain optical coherence tomography. *Opt Express* 2012; 20: 24925–24948.

22. Wang G, Guan C, Zhang X, et al. Precision control of piezo-actuated optical deflector with nonlinearity correction based on hysteresis model. *Opt Laser Technol* 2014; 57: 26–31.